PCCP

Accepted Manuscript

ROYAL SOCIETY OF CHEMISTRY

www.rsc.org/pccp

ARTICLE TYPE www. rsc.org/xxxxxx | XXXXXXXX

Solvation chemical shifts of perylenic antenna molecules from molecular dynamics simulations†

Nergiz Özcan,*[a] Jiří Mareš,[b], Dage Sundholm,[a] and Juha Vaara *[b]

Received Xth XXXXXXXXXX 20XX, Accepted Xth XXXXXXXXX 20XX
First published on the web Xth XXXXXXXXXX 200X
DOI: 10.1039/b000000x

Solvation-induced shifts in molecular properties can be realistically simulated by employing a dynamic model with explicit solvent molecules. In this work, ^{13}C NMR chemical shifts of various candidate antenna molecules for dye-sensitised solar cells have been studied by using density-functional theory calculations both *in vacuo* and by employing a dynamic solvation model. The solvent effects were investigated using instantaneous molecular dynamics snapshots containing the antenna molecule and surrounding acetonitrile solvent molecules. Such calculations take into account the main mechanisms of solvation-induced chemical shifts. We have analysed the contributions to the solvent shift due to the solvent susceptibility anisotropy, changes in the density of the virtual orbital space and the accessibility of the excited states to the pronouncedly local magnetic hyperfine operator. We present Lorentzian-broadened chemical shift stick spectra in which a comparison of the *in vacuo* and dynamic-solvation model results are graphically illustrated. The results show that the solvent-accessible atoms at the perimeter of the solute are influenced by the virtual states of the solvent molecules, which are visible to the hyperfine operators of the perimeter nuclei. This enables efficient coupling of the ground state of the solute to the magnetically allowed excited states, resulting in a positive chemical shift contribution of the perimeter nuclei. As a result of solvation, the chemical shift signals of perimeter nuclei are found to be displaced towards larger chemical shift values, whereas the nuclei of the inner region of the solute molecules show the opposite trend. The solvent susceptibility anisotropy is found to cause a small and practically constant contribution.

1 Introduction

Nuclear magnetic resonance (NMR) observables are sensitive to the environment of the nuclei and provide, consequently, valuable, high-resolution (atomically localised) structural information.[1] NMR spectroscopy can also be used for studying solvation effects, particularly for thoroughly monitoring the solvent-induced changes in the molecular electronic structure, because the NMR parameters are very sensitive to the interactions with the surrounding solvent molecules. Experimental NMR spectroscopy in combination with first principles computations can be used for interpreting and rationalising the underlying mechanisms of the solvent-induced effects on molecular magnetic properties.[2–4] In the early paper by Buckingham, Schaefer and Schneider,[5] NMR solvent effects originating from various interactions were formally analysed. Solvent effects on NMR parameters have also been investigated by using molecular dynamics (MD) simulation techniques, which incorporate the interaction of explicit solvent molecules with the solute. In particular, water as both the solvent and the solute has been simulated of in a number of studies.[6–11] For transition metal complexes, solvent effects on the NMR parameters such as the NMR chemical shifts and electric field gradients have also been studied computationally using MD simulations with explicit water molecules as solvent.[12] Solvent-induced shifts of electron paramagnetic resonance parameters have also been assessed by performing MD simulations.[13] In another study, ^{129}Xe NMR chemical shifts were investigated in the presence of benzene as explicit solvent.[14]

Comparison of NMR solvent shifts based on MD simulations, using explicit solvent molecules, with shifts calculated using implicit solvent models such as the polarizable continuum model (PCM)[15] and the Conductor-like Screening Model (COSMO),[3] show the importance of using dynamic solvation models with explicit solvent molecules, in realistic calculations of NMR properties.[16] Implicit solvation models are not able to accurately account for solvation effects on localised NMR properties due to explicit solute-solvent interactions such as formation of hydrogen bonds and van der Waals interaction. Another challenging mechanism for implicit sol-

† Electronic Supplementary Information (ESI) available: Tabulated ^{13}C NMR chemical shift values of each antenna model. Tabulated singlet excited state energies for three dynamic solvation snapshots of perylene. Tabulated singlet excited state energies of perylene and acetonitrile *in vacuo*. The .xyz coordinates of the perylene snapshots 103, 457 and 735.
See DOI: 10.1039/b000000x/

[a] *Department of Chemistry, P.O. Box 50, FIN-00014 University of Helsinki, Finland. Fax: 358-9-191 50169; Tel: +358-50-448 5733; E-mail: nergiz.ozcan@helsinki.fi*
[b] *NMR Research Group, Department of Physics, P.O. Box 3000, FIN-90014 University of Oulu, Finland. Fax: +358-8-553 1287; Tel: +358-40-196 6658; E-mail: juha.vaara@iki.fi*

vation models arises from magnetically induced currents in the solvent molecules, which can also affect the chemical shifts of the solute atoms.[17] Therefore, implicit models are of limited utility for simulating the influence of the solvent on the NMR chemical shifts.[18] However, they have been very successful in describing solvation energetics and other global molecular properties.[19,20]

The interaction of the solute with the solvent molecules alters the frontier orbital energies. In particular, the energy gap between the highest occupied molecular orbital (HOMO) and the lowest unoccupied molecular orbital (LUMO) is often lowered. This leads to smaller excitation energies that affect second-order molecular properties via the energy denominator, such as in the expression for the paramagnetic contribution to NMR nuclear shieldings (*vide infra*).

Solvation effects on NMR chemical shifts can be qualitatively examined in terms of the changes in the paramagnetic shielding, which include two kinds of influences. The indirect effects result from the changes in the atomic coordinates of the solute as well as the orientation and position of the solvent molecules relative to the solute. The direct polarization effects, on the other hand, do not need to involve any changes in the atomic structure but arise from changes in the electronic structure that affect the NMR chemical shifts.[21] Both the direct and indirect contributions to the solvent-induced shifts are incorporated in quantum-chemically sampled MD modelling using explicit and flexible solvent molecules.[22]

The aim of this work is to computationally investigate solvent effects on NMR chemical shifts for more complicated molecular systems than liquid water. Here we have performed NMR chemical shift calculations on nine different perylenic dye molecules, which are candidate pigment molecules for use in solar cells, where they are attached to a TiO_2 (anatase) surface immersed in acetonitrile, CH_3CN.[23] From the computational point of view, acetonitrile is an interesting solvent, because it possesses both a strong electric dipole moment and large magnetisability anisotropy due to -C ≡N group.

In this work, we used these dye molecules to study the solvation effects on localised NMR properties. We employed density-functional theory (DFT) in the calculations of NMR shifts both *in vacuo* and in a dynamic solvation model where the antenna candidates are surrounded by explicit solvent (acetonitrile) molecules in instantaneous configurations sampled from MD trajectories. We performed quantum-mechanical calculations using DFT for snapshots that consist of the dye molecule and a finite-thickness CH_3CN solvent shell. Subsequently, a statistical average of the NMR chemical shifts over these snapshots was calculated.

We report solvent effects for the ^{13}C NMR chemical shifts of the dye molecules and focus on the different situations of the solvent-accessible nuclei at the perimeter of these largely planar perylenes, as well as the carbons closer to the center of the molecules. The solvation shifts are analysed, first, in terms of anisotropy of the solvent susceptibility and, secondly, as a result of changes in the molecular electronic structure. We investigate the latter aspect in terms of excitation energies and the coupling of the magnetically allowed excited states to the ground state, relevant for the orbital Zeeman (OZ) interaction with the magnetic field, and the localised orbital hyperfine (paramagnetic nuclear spin-electron orbit, PSO) operator.

In our analysis, magnetic-dipole allowed excited states were calculated for both the *in vacuo* situation and a few selected snapshots of the dynamic, explicitly solvated model of the simplest present perylene, to elucidate the general trends in the NMR solvation shifts for all the present antenna molecules. We express the calculated shifts in terms of colour-coded (according to the sign and magnitude of the solvation shift), Lorentzian-broadened chemical shift spectra, as well as additional density-of-states (DOS) figures and magnetically allowed absorption spectra.

2 Theory

The NMR chemical shift is obtained from the difference between the shielding constants of the reference compound and the nucleus of interest;

$$\delta = \sigma_{\mathrm{ref}} - \sigma. \tag{1}$$

The Cartesian $\varepsilon\tau$ component of the nuclear shielding tensor

$$\sigma_{\varepsilon\tau} = \frac{1}{\gamma\hbar}\frac{\partial^2 E}{\partial B_\varepsilon \partial I_\tau} \tag{2}$$

can be determined as the second derivative of the molecular energy E with respect to the components of the applied external magnetic field $\boldsymbol{B}$ and the nuclear magnetic moment μ, which is proportional to the nuclear spin $\boldsymbol{I}$ as $\boldsymbol{\mu} = \gamma\hbar\boldsymbol{I}$ where γ is the gyromagnetic ratio.[24] At the nonrelativistic level of theory, which is well applicable to the present systems that consist of only light atoms, the shielding tensor can be formally written as a sum of the diamagnetic and paramagnetic parts[25,26]

$$\sigma_{\varepsilon\tau} = \sigma^d_{\varepsilon\tau} + \sigma^p_{\varepsilon\tau}. \tag{3}$$

The total shielding relative to a given reference [Eq. 1] is the experimental observable, whereas the detailed division into the dia- and paramagnetic contributions depends on the choice of the gauge origin for the magnetic vector potential.[27]

The diamagnetic contribution to the shielding constant is related to the electron density at the nucleus in question. Therefore, different diamagnetic chemical shifts are obtained, e.g., between situations where the investigated atom is bonded to partners that have different electronegativity. More often, however, it is the paramagnetic contribution to the chemical shift that features the largest sensitivity to the chemical

environment of the nucleus. Ramsey showed that the paramagnetic shielding can be calculated using a second-order perturbation-theoretical expression involving the OZ and PSO operators[25,26]

$$\sigma^p_{\varepsilon\tau} = \frac{\alpha^2}{2}\left[\sum_m \frac{\langle 0|h^{\mathrm{OZ}}_\varepsilon|m\rangle\langle m|h^{\mathrm{PSO}}_\tau|0\rangle}{E_0 - E_m} + c.c.\right], \qquad (4)$$

where α is the fine structure constant and E_0 and E_m are the ground and excited state energies, respectively. The expression shows that low-lying excited states that are symmetry accessible for the magnetic operators, are likely to dominate the paramagnetic contribution to the nuclear shielding.

It was shown by Buckingham *et al.* that the solvent-induced nuclear shielding can formally be divided into a sum of four contributions[5]

$$\sigma_{\mathrm{sol}} = \sigma_{\mathrm{bulk}} + \sigma_a + \sigma_W + \sigma_E, \qquad (5)$$

where σ_{bulk} is the contribution from bulk magnetic susceptibility of the solution, σ_a is due to the anisotropy of the susceptibility (magnetisability) of the solvent, σ_W arises from the van der Waals interaction between the solute and the solvent, and σ_E from the polarisation effects resulting from electric fields due to the solvent. In modern experiments, the contribution from the bulk magnetic susceptibility vanishes due to the use of an internal chemical shift reference. In conventional DFT calculations, such as the ones carried out in the present paper, the van der Waals contribution cannot be captured. On the other hand, with polar solvents such as acetonitrile, the electrostatic contribution is assumed to dominate the solvation shifts, and this can be expected to be well-reproduced by DFT.

In this paper, solvent-induced chemical shifts are analysed in terms of two contributions. One of these is the solvent effect, δ_a, which arises from the magnetic anisotropy of the CH_3CN solvent molecules, specifically due to the magnetically induced currents around the multiple bond of the -C≡N group. The δ_a term turns out to represent a small and fairly constant contribution to the ^{13}C NMR chemical shifts in the present systems. It arises from the secondary magnetic field that is created by the induced magnetic moment and results in a negative contribution to the shielding of the neighbouring solute nucleus and, therefore it increases the chemical shift. This contribution is included naturally in the DFT shielding calculations carried out on explicitly solvated simulation snapshots. Its magnitude can be *a posteriori* extracted from the calculated DFT shifts. This is done by calculating magnetizability anisotropy $\Delta\chi_g$ of CH_3CN at the DFT level and then applying the equation given in Ref.[28],

$$\sigma_a = -\langle \frac{1}{6\pi r^3}\Delta\chi_g\rangle \qquad (6)$$

to obtain the δ_a shift contribution. Here, r is the distance between the nucleus under study and the -C≡N group of the solvent molecule, and the angular brackets denote time and ensemble averaging. We present results for the solvation-induced chemical shifts both with and without the δ_a contribution.

A more important contribution to the solvation shifts arises due to solvent-induced changes in the molecular electronic structure. These changes are mainly included in Buckingham's σ_E term, and comprise both indirect and direct solvation effects *vide supra*. One of the underlying factors is the arrangement of both the solute and the solvent molecules in order to minimise the total energy. The situation where the solute molecule is surrounded by the explicit solvent in a shell of given thickness stabilises in most cases the ground state relatively to the excited states. However, in some cases the solvent molecules might stabilise the excited levels relatively to the ground state. Thus, the gap between the ground state and excited states generally becomes smaller and more rarely larger than for the molecule *in vacuo*. The DOS of the virtual orbitals increases due to the presence of explicit solvent molecules. These changes in the electronic states are monitored using DOS figures in the following.

The results are interpreted in terms of the amplitudes and localisation of the excited states that couple to the ground state through the magnetic operators as indicated by Eq. (4), which suggests that nuclei are less shielded (as the sign of σ^p is negative) when the coupling with the excited state is strong. The strong local nature of the PSO operator implies that a large amplitude of magnetically allowed excited states at the nuclear site causes a large positive contribution to the chemical shift.

2.1 Calculations

2.1.1 Antenna molecules. The considered antenna molecules are shown in Fig. 1. The molecules are perylene (model I), P-anhydride (model H), P-anhydride-N(Me)$_2$ (model G), P-anhydride-NPh$_2$ (model F), P-anhydride-(SMe)$_2$ (model E), P-anhydride-(SPh)$_2$ (model D), P-anhydride-(SMe)$_2$-N(Me)$_2$ (model C), P-anhydride-(SPh)$_2$-NPh$_2$ (model B) and P-anhydride-(SPh)$_2$-N(PhR)$_2$ (model A).[29] The abbreviations used in the names of the antennas molecules correspond to Ph=phenyl, R=2-dimethyl-4-methyl-pentane, P= perylene and Me=methyl.

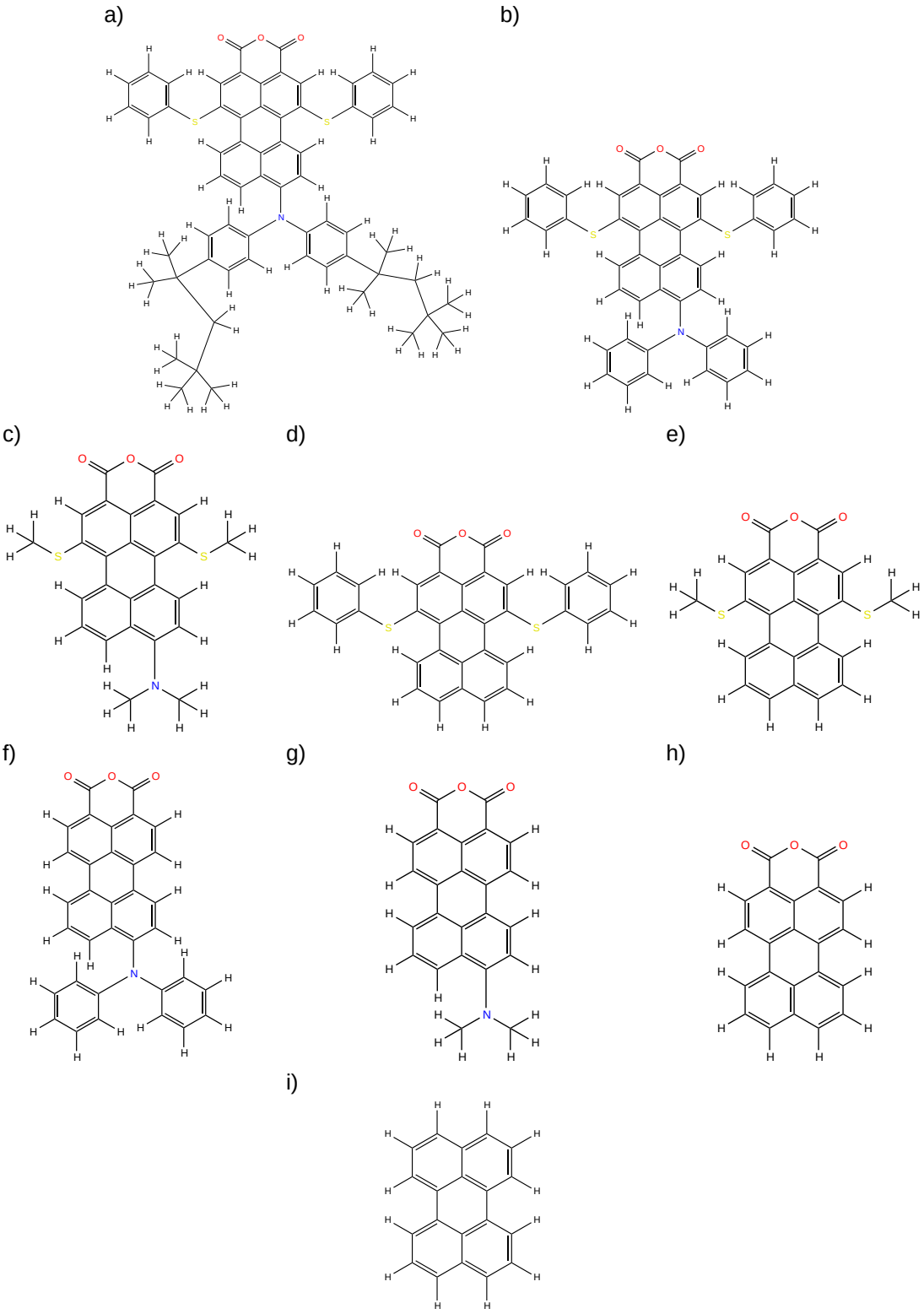

Fig. 1 The studied antenna candidate molecules: a) model A, b) model B, c) model C, d) model D, e) model E, f) model F, g) model G, h) model H and i) perylene (model I).

2.1.2 Technical details of the simulations. The parameterisation of the photomolecules used the GAFF forcefield of the antechamber[30] suite of AMBER 12.[31] The partial charges were fitted from a semiempirical AM1[32] calculation (the "bcc" option for the charge method of antechamber was used). The molecules were solvated in acetonitrile, for which the parameterisation of Ref.[33] was used. The simulation boxes contain different numbers of solvent molecules ranging from 285 for the smallest antenna model to 565 molecules for the largest model. All the MD simulations were performed using the NAMD software.[34] After 0.5 ns of equilibration at 300 K and 1 atm in the constant pressure and temperature *NPT* ensemble, 1.5 ns of production trajectory was obtained in the same conditions. The MD integration step was 1 fs.

For the QC calculation of MD snapshots, clusters containing of the antenna molecule with a shell of solvent were extracted. Into the solvation shell of a given snapshot we selected the molecules that have at least one atom closer than a given distance from any atom of the solute molecule. Fig. 2 shows an example snapshot of perylene with CH_3CN solvent molecules in a shell of 3.5 Å thickness.

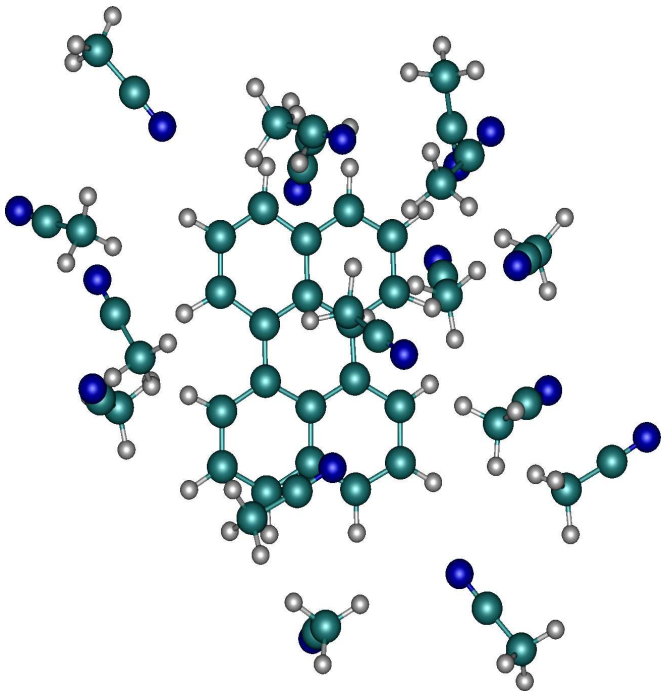

Fig. 2 A cluster constructed from a single snapshot of a molecular dynamics trajectory: Perylene with explicit CH_3CN solvent in a 3.5 Å thick shell.

2.1.3 Quantum-chemical calculations. The *in vacuo* structures of the investigated photomolecules were obtained from optimisations carried out in Ref.[29] at the B3LYP level[35–37] using the def2-TZVP basis sets.[38] For solvation effects we average over the chemical shifts calculated for a number of snapshots spaced evenly in time, throughout the equilibrated part of each trajectory. A snapshot was picked for the quantum-chemical calculations in 8 ps intervals for models A and B and in 16 ps intervals for the other systems. The total number of snapshots that were used for the averaging was 188 for models A and B and 94 for the other antenna models.

We calculated the statistical errors of the averages by the data halving method of Flyvbjerg and Petersen.[39] Fig. 3 shows the running averages of the 94 snapshots for six chosen nuclei belonging to different groups of perylene (model I). Calculations of ^{13}C NMR chemical shifts were performed at the B3LYP/def2-SVP[40] level. The CH_4 molecule was used as the chemical shift reference system with the shielding value of σ_C = 195.62 ppm at the B3LYP/def2-SVP level.

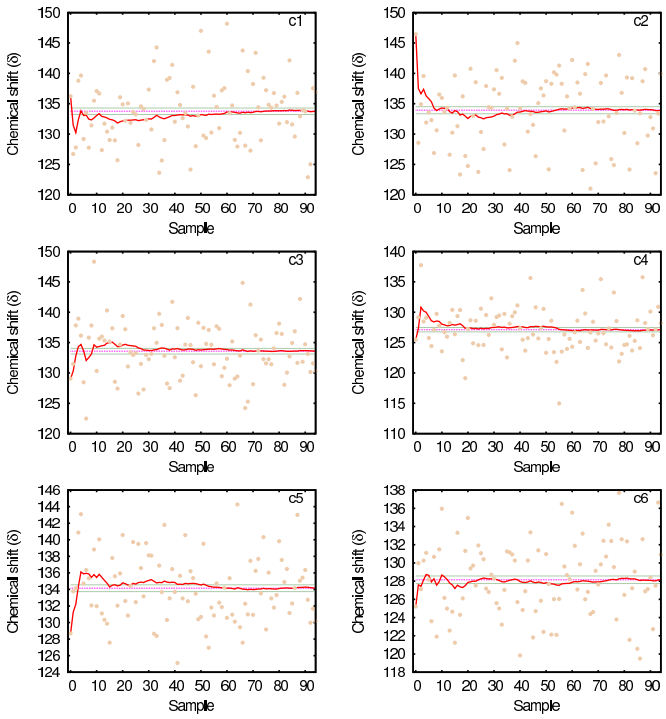

Fig. 3 Running averages of the chemical shifts (ppm) of the nuclei C1, C2, C3, C4, C5 and C6 of perylene. Each nucleus belongs to a different group of equivalent nuclei, G1, G2, G3, G4, G5 and G6, as shown in Fig. 5 below. The horizontal red and blue lines denote the average and its statistical error margins, respectively.

The chemical shifts of the equivalent nuclei were averaged over and a common shift value is reported for them for all the antennas. Each molecule contains number of nuclei that have equivalent chemical shifts either under the point group operations of the *in vacuo* structure, or based on the practical chemical equivalence in the solution phase at the experimental temperature. Those nuclei are reported in Table 1 and the

Tables S1–S8 (in the ESI), which list the calculated chemical shifts of each system. All the nuclear magnetic shielding calculations were performed with TURBOMOLE 6.4 package.[41] It should be noted here that the present MD sampling is not extensive enough for entirely quantitative results, and a longer MD trajectory as well as increased quantum-mechanical sampling would be needed for that purpose.[42] In the present paper we focus on the qualitative trends in the solvated shifts of different non-equivalent nuclei.

Table 1 Calculated ^{13}C NMR chemical shifts (ppm) in perylene. The results are presented for groups of equivalent nuclei. The B3LYP/def2-SVP level of theory was used

Group[a]	$\delta_{in\ vacuo}$	δ_{sol}	δ_a	$\delta_{\mathrm{sol}} - \delta_a$	$\delta_{\mathrm{sol}} - \delta_{in\ vacuo}$
G1	138.87	131.85	-0.85	132.70	-7.02
G2	133.45	126.74	-0.81	127.54	-6.72
G3	136.98	134.92	-0.83	135.75	-2.06
G4	130.48	134.39	-0.92	135.31	3.90
G5	122.74	127.33	-0.91	128.24	4.59
G6	128.20	133.28	-0.94	134.22	5.08

[a] See Fig. 5.

Excitation energy calculations were performed for perylene *in vacuo* and in three explicitly solvated MD snapshots, which possess a low potential energy. We calculated the magnetically relevant singlet excited state energies together with the magnetic transition dipole moments at the B3LYP/def2-SVP level. The results are represented as magnetic absorption spectra based on the squared magnetic dipole transition moment values of each calculated excited state.

3 Results and Discussion

3.1 Comparison of methods

We first compare the Hartree-Fock (HF) and various DFT methods in the calculation of the ^{13}C NMR chemical shifts of perylene. Fig. 4 shows the results at different levels for the *in vacuo* model. These calculations were performed using the def2-SVP basis set. No considerable difference can be seen among the methods. The exact exchange admixture (BLYP: 0%; B3LYP: 20%; BHandHLYP: 50%) has been found to be the most important characteristic of the DFT functionals from the point of view of NMR parameters.[43] The presently obtained, very similar data for the different functionals suggest that it is safe to pursue the further calculations of this paper with the standard B3LYP functional. The calculated chemical shifts can be found in Table S9 in the ESI.

The calibration of different basis sets and thickness of the explicit solvation shell was performed with test calculations on one of the candidate antennas, model B. We compared the

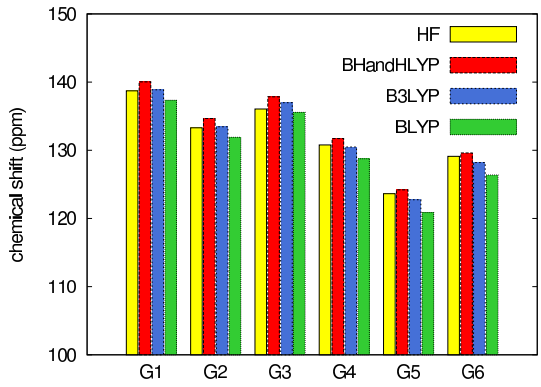

Fig. 4 Perylene ^{13}C NMR chemical shifts (ppm) calculated with different methods and the def2-SVP basis set. The *in vacuo* model was used. The numbering of groups of equivalent nuclei is shown in Fig. 5.

results obtained with def2-SVP and def2-TZVP basis sets in shells with 3.5 and 5.0 Å thicknesses. The results are listed in Table S10 in the ESI. The difference of the explicit solvation shell thicknesses causes changes of about 0.11 ppm on the chemical shifts, as calculated at the def2-SVP level. On the basis of the results of the test, the production calculations were performed with a 3.5 Å thick shell.

About 10 ppm larger chemical shifts are obtained with the larger def2-TZVP basis with 3.5 Å shell thickness, as compared to the def2-SVP basis. While the smaller def2-SVP basis sets represents a compromise for obtained chemical shift values, our principal goal is in the qualitative analysis of the trends of the solvation shifts. For this purpose, the def2-SVP basis is sufficient and computationally feasible. Overall, the B3LYP method together with the 3.5 Å explicit solvation shell thickness and the def2-SVP basis set was chosen for dynamic solvation calculations. We will principally use the simplest present system, perylene, to analyse and depict the chemical shift trends in the present antenna molecules. We present the calculated ^{13}C NMR chemical shift results in three groups of antennas with increasing size and complexity.

3.2 Perylene

The calculated chemical shifts for perylene are listed in Table 1. We present both the *in vacuo* and solvation δ_{sol} chemical shifts, together with the solvent anisotropic magnetisability contribution δ_a in the third column. The solvation chemical shifts without this *a posteriori* extracted contribution, $\delta_{\mathrm{sol}} - \delta_a$, are also listed in the fourth column. In the last column, the total difference $\delta_{\mathrm{sol}} - \delta_{in\ vacuo}$ between the solvated and the *in vacuo* situations is given. This is represented with colour-coding in both the chemical shift stick spectra and the corresponding figure of the system, in Fig. 5. The overall

scale of the solvation-induced changes shows both the positive and negative differences that represent increase and decrease of the ^{13}C shifts as a result of applying the dynamic solvation model, as compared to the *in vacuo* model. The ^{13}C shifts that have smaller values in the dynamic solvation model than *in vacuo* are indicated with red colour. These signals move to right in the chemical shift spectra of the dynamic solvation model. The blue signals represent positive changes; their chemical shifts increase in the dynamic solvation model as compared to the *in vacuo* situation. For simplicity, nuclei other than carbon are omitted from the Figure.

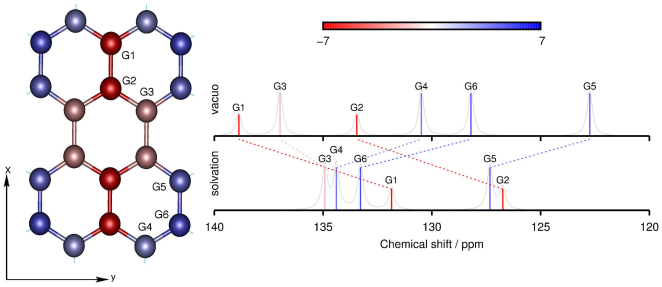

Fig. 5 Calculated chemical shift stick spectra of perylene as well as its colour-coded structure. The chemical shifts of the equivalent nuclei are averaged over and reported as group results. The color coding both in the stick spectra and the structure represents the changes in the chemical shifts upon solvation. The red-white-blue scale indicates a decrease (red) and an increase (blue) of the chemical shifts, when changing from the *in vacuo* model to the averaged, explicit solvated calculations. See the text for a detailed explanation.

Fig. 5 shows a clear division into the red signals (decreased chemical shifts) from the inner part of the system and blue signals (shift increase) from the solvent-accessible perimeter atoms. As a result, in the dynamic solvation model the total chemical shift range is significantly smaller than *in vacuo*. The chemical shifts of the nuclei are seen to change in a certain way depending on the location of the nuclei in the system. Although there are no experimental data available for the present systems yet, our findings correlate well with the earlier experimental study on hydrocarbons by Abboud *et al.*[44]

In the following section, the chemical shift trends in perylene will be analysed in terms of excited states and the coupling of the ground state to these excited states through the magnetic operators. Due to the locality of the PSO hyperfine operator, solvation-induced changes can be expected on the solvent-accessible perimeter regions of the solute. On the other hand, through solvation-induced changes in the localisation of the magnetically allowed excited states of the solute, also the shifts of the inner, not directly solvent-accessible nuclei, can change.

3.2.1 Analysis of the results. Fig. 6 shows the total DOS in the immediate vicinity of the HOMO-LUMO gap of perylene in the *in vacuo* and three representative, explicitly solvated snapshots extracted from the MD simulation. For the latter purpose, we chose the snapshots numbers 103, 457 and 753 which have a low potential energy in the MD simulations of the dynamic solvation model. The coordinates of these snapshots can be found in the ESI. The aim is to capture the changes in the molecular electronic structure occurring upon solvation, by monitoring the DOS of each model.

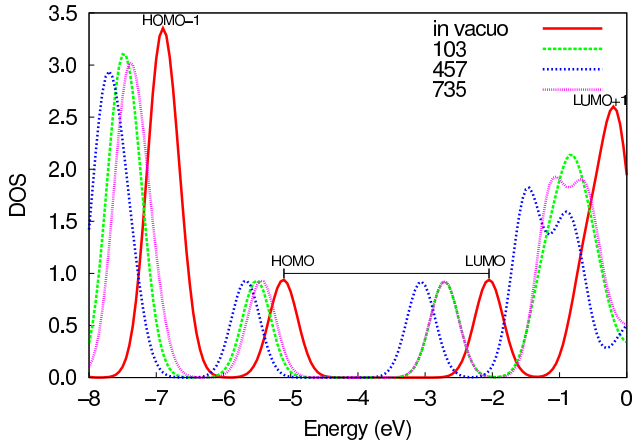

Fig. 6 Calculated (B3LYP/def2-SVP) density-of-states diagram for perylene (model I) *in vacuo* and in three explicitly solvated molecular dynamics snapshot structures (snapshot numbers 103, 457 and 735). A Gaussian function with the half-width parameter equal to 0.5 eV has been used to broaden the individual molecular orbital energy levels.

The first effect that can be seen is the stabilisation of the occupied orbital energy levels. As compared to the *in vacuo* model, the energies of the occupied molecular orbitals of the solvation models are lowered, all the way up to the HOMO. Similarly to the occupied orbitals, the energies of the virtual orbitals also decrease, even by a larger amount. Hence, the HOMO-LUMO gap is also smaller for all three solvated snapshots as compared to *in vacuo*. Another important feature is that the LUMO+1 region in the solvated snapshots is, besides lowered in energy, also broadened as compared to the *in vacuo* case. These features suggest that the valence excitation energies decrease in the solvation model. This is important in order to understand the behaviour of the chemical shift signals in perylene in terms of magnetic coupling to excited states.

We will next look at the magnetic coupling, specifically via the OZ operator h^{OZ}, to the excited states of perylene in more detail. This is done by calculating the magnetic dipole transition moments $\boldsymbol{\mu}_{0m} \propto \langle 0|\boldsymbol{h}^{\mathrm{OZ}}|m\rangle$ from the ground state to the excited states. In order to have a consistent comparison between the *in vacuo* and solvation models, we rotate the instan-

taneous snapshot structures to the Eckart frame[45,46] coinciding with the *in vacuo* perylene at its equilibrium structure. In this way, both the *in vacuo* and solvated structures have their $\boldsymbol{\mu}_{0m}$ expressed in a common coordinate frame and we can capture clearly the solvation effects on the Cartesian components $\mu^2_{0m,x}$, $\mu^2_{0m,y}$ and $\mu^2_{0m,z}$, in specific directions in the quite rigid perylene structure.

We illustrate the excited-state calculations of both the *in vacuo* and the three dynamic-solvation models as "magnetic absorption spectra", in Fig. 7. The excitation bands of the CH_3CN solvent molecules start at clearly higher energies than those of the solute, at about 7.95 eV.

As the main interest here is in qualitative analysis of the paramagnetic chemical shifts in terms of low-lying excited states, the excitation energy calculations were performed by the same DFT/B3LYP functional and def2-SVP basis set as in the calculations of NMR nuclear shielding. However, based on the previous studies,[47–49] we limited the spectral range up to the negative of the orbital energy of the highest occupied orbital, $-e(\mathrm{HOMO})$ equal to 5.11, 5.51, 5.67 and 5.43 eV for the *in vacuo* situation as well as snapshots number 103, 457 and 735, respectively, in order to avoid the errors due to the DFT method used. The calculated excited state energies can be found in the Tables S11-S12 in the ESI.

We focus on the changes of the solute excitations upon solvation. The spectra consist of peaks the intensities of which are proportional to $\mu^2_{0m,x}$, $\mu^2_{0m,y}$ and $\mu^2_{0m,z}$. The spectra show the lowest singlet, magnetically allowed, excited states belonging to the B_{1g}, B_{2g} and B_{3g} irreps of the *in vacuo* model with D_{2h} symmetry. The integrated intensities corresponding to Fig. 7 are given in Fig. 8.

Figures 7 and 8 indicate a lowering of magnetically allowed excited states induced by solvation, in agreement with what could be inferred from the DOS images. At the same time, the negatively signed, paramagnetic nuclear shielding contributions can be expected to become stronger. However, the solvation-induced changes are seen to affect differently located ^{13}C nuclei in quite different ways, as seen in Fig. 5. The perimeter solute nuclei become less shielded due to the solvation-induced changes in the excited states and therefore their chemical shift values increase. Solvation has introduced a stronger coupling of these excited states with the ground state through the PSO operator in Equation 4. On the other hand, chemical shifts of the innermost, less solvent-accessible nuclei experience the opposite change, a decrease upon solvation. The site-specificity of the solvation effects suggest changes in the localisation of the magnetically accessible excited states, which are then reflected in the transition matrix elements $\langle m|h^{\mathrm{PSO}}_{\tau}|0\rangle$ of the pronouncedly local PSO operator.

Fig. 9 shows the difference densities of the five lowest, magnetically allowed singlet excited states from the ground state. The excitations take place mostly in the central region of the

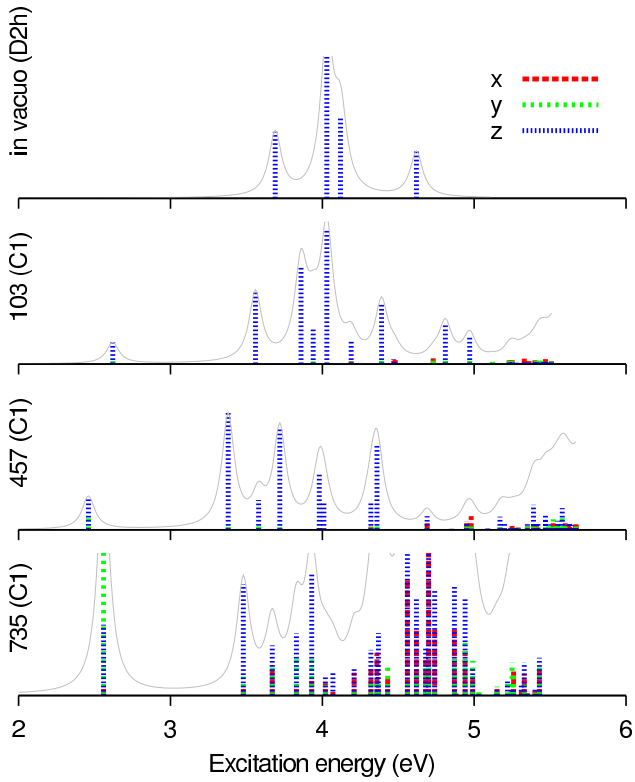

Fig. 7 Magnetic absorption spectra based on calculations of the squared magnetic dipole transition moment $\mu^2_{0m} = \mu^2_{0m,x} + \mu^2_{0m,y} + \mu^2_{0m,z}$ between the ground and excited states of perylene, in the *in vacuo* and three explicitly solvated molecular dynamics snapshots (snapshots 103, 457 and 735), calculated at the B3LYP/def2-SVP level. The Lorentzian-broadened spectra are shown with the full width at half-maximum equal to 0.7 ppm. The *x*, *y* and *z* components are represented by red, green and blue colors, respectively. The *x*, *y* and *z* directions are specified in the molecular frame in Fig. 5.

molecule in the *in vacuo* structure. This results in the nuclei at the center of the system to be less shielded, particularly in the off-plane *zz*-components of the shielding tensors, than the perimeter nuclei. With solvation, the weight of the low-lying excited states moves towards the perimeter. This means that the center atoms become more shielded and are, hence, marked with red in the stick spectra of Fig. 5. On the other hand, the fact that the excitations increasingly take place at the perimeter region of the system in the explicitly solvated snapshots, as compared to the *in vacuo* situation, allows a stronger coupling to the excited states, through the PSO operator. This causes the nuclei to become less shielded in the perimeter regions, explaining why the perimeter signals move to larger chemical shifts and are marked with blue in Fig. 5.

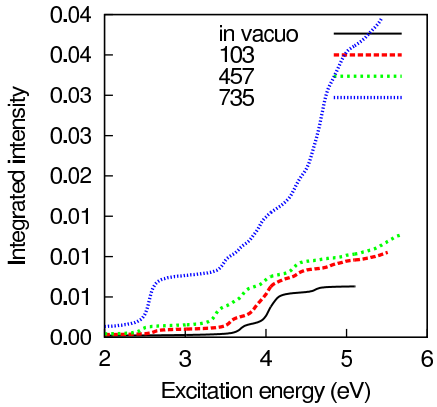

Fig. 8 Integrated intensity $\int_0^{E_{exc}} \mu_{0m}^2(E)\,\mathrm{d}E$ corresponding to the calculated square of the transition dipole moment μ_{0m}^2 between the ground and excited states of perylene. Both the *in vacuo* and three low-energy instantaneous, explicitly solvated snapshots (numbers 103, 457 and 735) are illustrated.

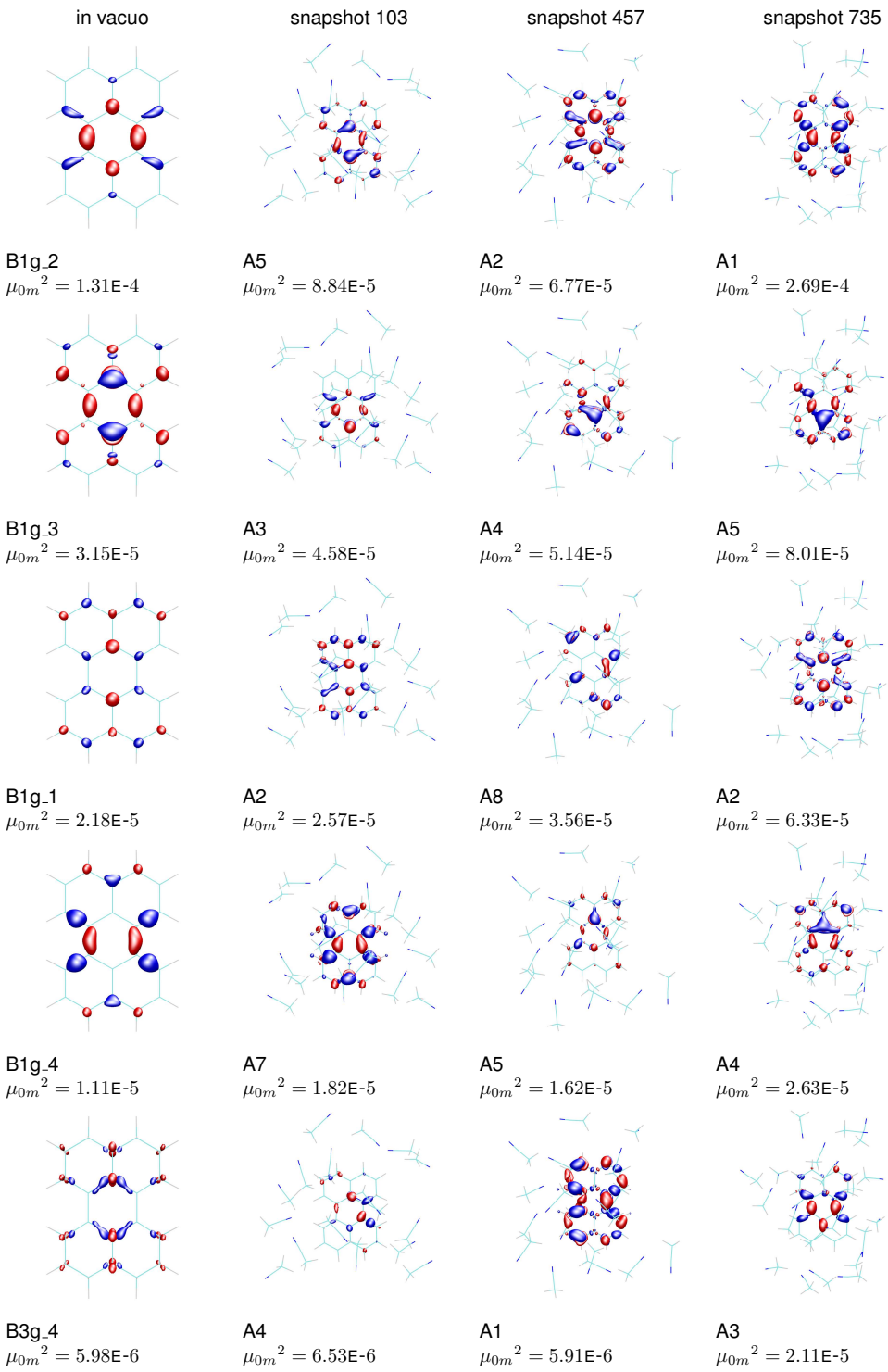

Fig. 9 Difference densities for the perylene molecule between five low-lying magnetically most relevant excited states and the ground state of the *in vacuo* structure and three explicitly solvated molecular dynamics snapshots (numbers 103, 457 and 735). In the *in vacuo* case we show five states for the two magnetically allowed irreps B_{1g} and B_{3g}, corresponding to the magnetic transition dipole moment in the *z* and *x* directions, respectively. The blue and red coloring refer to build-up and depletion of density in the excited state as compared to ground state, respectively. The calculated excited state energies can be found in the Tables S11-S12 in Supporting Information.

3.3 Model H, model G and model F

In the remaining parts of the paper we present the calculated chemical shifts for the more complicated antenna candidates than our prototypic perylene system. We focus on the similarities and differences of the results as compared to the perylene case. The general characteristics of chemical shift spectra of the larger antenna models are very similar to perylene. The inner regions of the systems are red, indicating decrease in the chemical shift upon solvation, and the perimeter regions are blue, in accordance with the analysis performed for perylene. The solvation-induced changes occur on a broader shift range in these larger molecules than in perylene.

The situation for the first three, larger antenna models is illustrated in Fig. 10. The signals that are the most deshielded, located at the high end of the chemical shift scale belong to atomic centers that are bonded to two oxygens. This is contributed to by to the high electronegativity of oxygen, which diminishes the electron density at the carbons and causes their deshielding via the reduced, positive diamagnetic contribution. These nuclei perform similarly to the perimeter centers upon solvation, *i.e.*, their chemical shifts increase due to the enhanced paramagnetic shielding contribution.

The nuclei of the methyl groups (model G) display different chemical shift characteristics as compared to those of the phenyl groups (model F). The signal from the G1 nuclei in the methyl groups of model G is highly shielded and appears at the right-hand-side of the spectrum. The position of the signal is close to that for the chemical shift reference system CH_4. The methyl signals are fairly insensitive to the solvation-induced changes. The C4 center in the main body of model G, which is bonded to the electronegative nitrogen, has a large shift and behaves as an inside atom upon solvation.

The G1 nuclei of the phenyl groups in model F show the opposite characteristics as compared to the methyl group. The phenyl signal appears on the left-hand-side (large and positive chemical shift) of the spectrum. The solvent shift of the signals from C14 and G1 are similarly as the ”inside” atoms. The other signals from the phenyl group of model F (G2-G4) display a shift increase expected for solvent accessible nuclei. The C9 signal in model G and the C19 signal in model F have extremely large solvent shifts of 19.35 ppm and 10.54 ppm towards larger chemical shifts, respectively.

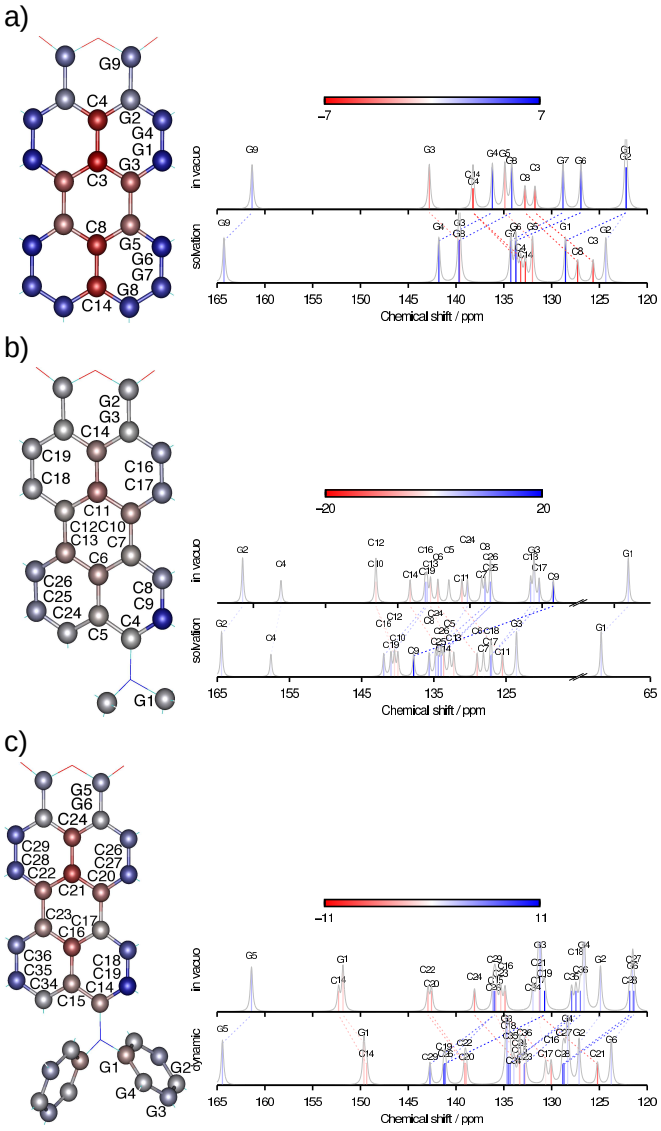

Fig. 10 Calculated ^{13}C NMR chemical shift stick spectra and color-coded structures of a) model H, b) model G and c) model F. See Fig. 5 for further explanations.

3.4 Model E, model D and model C

The colour-coded structures and chemical shift stick spectra of models C, D and E are given in Fig. 11. The general features of the carbons that are bonded to oxygen and nitrogen in these models are the same the as discussed above. The signals from the carbons located within the main body of the structures and bonded to sulphur, *i.e.*, G1 in model E and model D, as well as C3 and C13 in model C, are shifted by the solvent to smaller chemical shifts similar as interior carbons.

The -S-CH_3 methyl group (G7) in model E is not as inert to solvation as the G1 carbon in the -N-CH_3 of model G. The G9 signal of the phenyl group in model D is shifted to larger chemical shifts by the solvent. Thus, the behaviour of the G9 carbon that is bonded via a sulphur atom to the perylene differs from that of the G1 carbon in the phenyl group of model F, which is directly connected to the perylene moiety.

3.5 Model B and model A

Solvent effects on the ^{13}C NMR chemical shifts of the biggest studied chromophores can be analysed in terms of the previously discussed, smaller perylenes, as they share common characteristics (see Fig. 12). The signals of the -N-Ph phenyl substituent (G6) of models A and B are shifted by the solvent towards smaller chemical shifts, whereas the other sites of the -N-phenyl group are relatively insensitive to solvation as for the previously discussed F model. Surprisingly, the chemical shifts of the carbons of the -S-Ph group slightly decrease upon solvation in contrast to the trend for the corresponding nuclei of model D. The reason for the different solvent shifts is not understood. Apparently, it is caused via some mechanism by the bulky substituents of the A and B models.

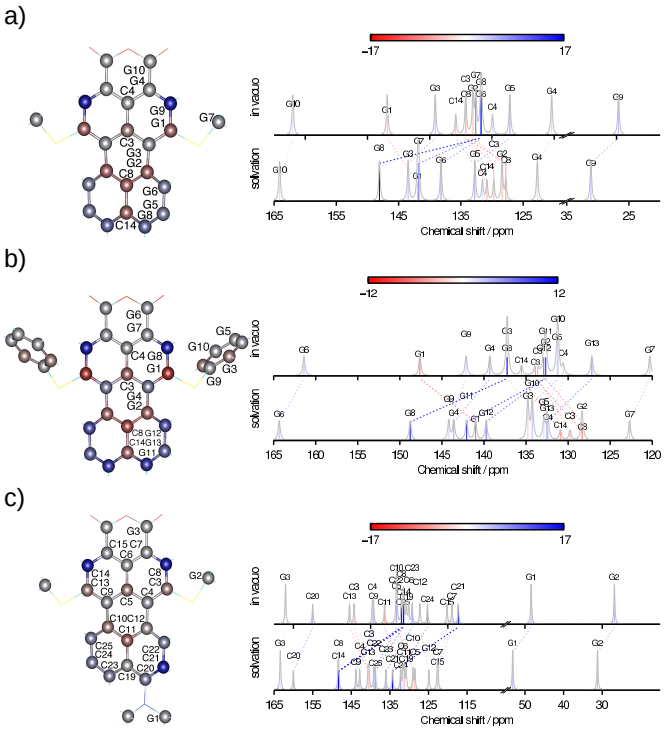

Fig. 11 Calculated ^{13}C NMR chemical shift stick spectra and colour-coded structures of a) model E, b) model D and c) model C. See Fig. 5 for further explanations.

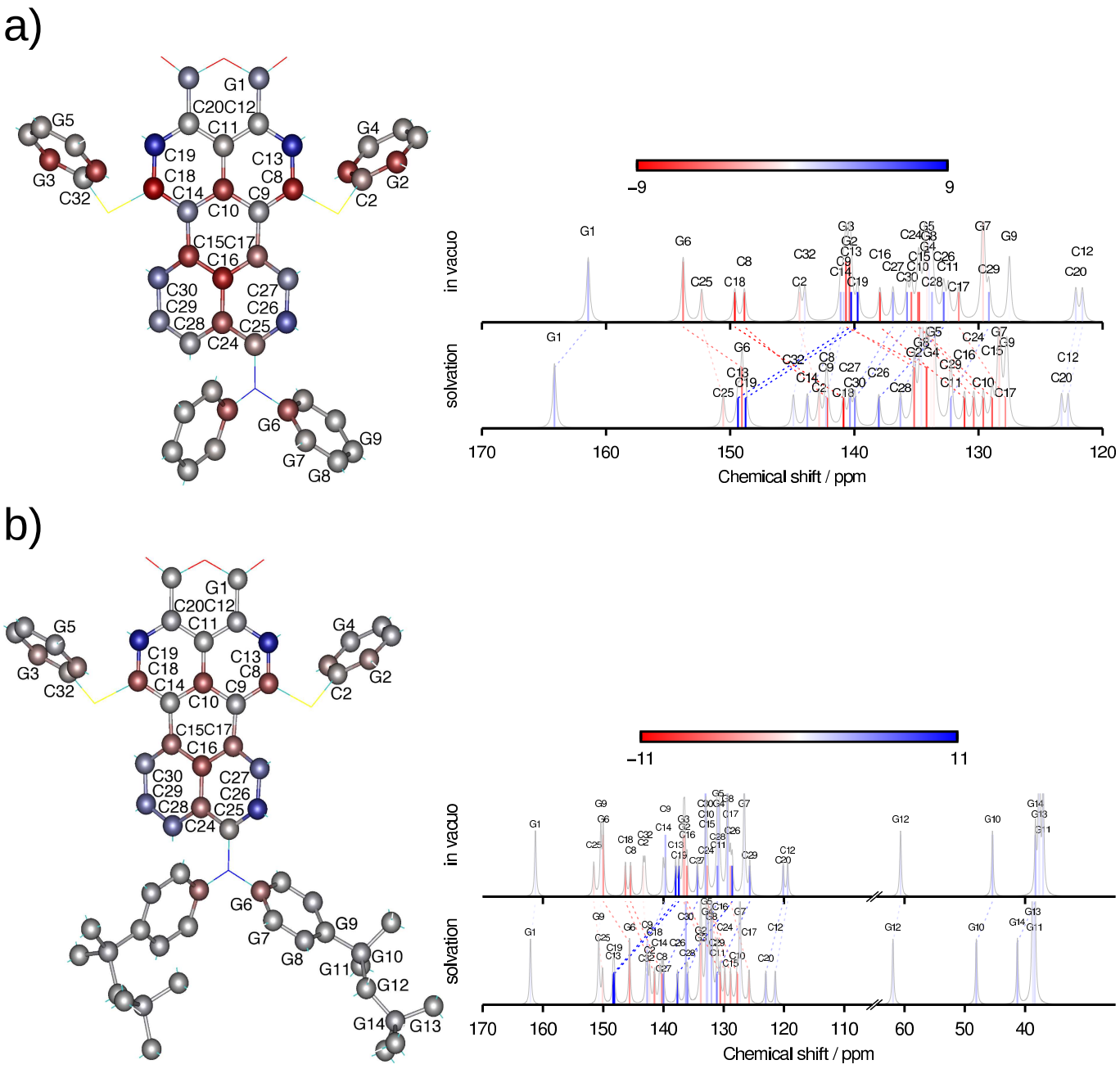

Fig. 12 Calculated ^{13}C NMR chemical shift stick spectra and colour-coded structures of a) model B and b) model A. See Fig. 5 for further explanations.

In model A, the signals from the nuclei belonging to G11-14 in the larger substituent appear on the right-hand-side of the spectrum, similar to signals of aliphatic hydrocarbons. This behaviour can be related to the sp^3-hybridized character of the substituent in question, resembling the methyl groups in the smaller models and the CH_4 reference system.

4 Conclusions

In calculations of NMR chemical shifts, modeling of solvent effects is challenging, because it is essential to explicitly include solvent molecules. The interactions between the solute and surrounding solvent molecules lead to solvent-induced changes of the shifts that are sensitive to the local environment of the nucleus of interest.

We have calculated the ^{13}C NMR chemical shifts of nine perylene-based chromophore molecules that might be used in solar cells. We present calculations on the molecules *in vacuo* and using a dynamic, explicit solvation model. The solvent-induced chemical shifts were analyzed in detail for perylene, which is the simplest studied antenna molecule. The trends of the chemical shifts of the larger antenna molecules with increasing complexity were interpreted based on the analysis performed for perylene. The dynamic solvation model was implemented in calculations where the antenna molecules were surrounded by a number of acetonitrile solvent molecule in 3.5 Å thick shell, sampled from MD simulation trajectories. The individual NMR calculations were performed for a number of snapshots for each molecule. The results of the dynamic solvation model were obtained by statistical averaging of the calculated nuclear shieldings obtained at the DFT level. We presented Lorentzian-broadened chemical shift stick spectra to illustrate the solvent induced changes on the chemical shifts. The results are also illustrated using a colour-coding that indicated decrease or increase of the chemical shifts upon solvation.

The results show that the chemical shifts of the ^{13}C nuclei respond differently to solvation depending on their location in the molecule. The interactions with the solvent molecules increase the chemical shifts of the solvent accessible nuclei at the molecular perimeter, whereas the signals from the central region show the opposite behaviour. The solvent effects of the chemical shifts are interpreted in terms of changes in the electronic structure of the molecules. The calculations show that the energies of the occupied and virtual orbital are significantly stabilized due to solvation. Calculations of the so-called magnetic absorption spectra revealed that the excited states of the solute are lowered in energy by solvation. The excited states become more accessible to the perimeter nuclei as well as less accessible for the central nuclei.

The paramagnetic contribution to nuclear shielding, resulting from Zeeman and PSO hyperfine operators, depends on the coupling between the ground state and the magnetically allowed excited states. A increase in the chemical shift indicates a stronger coupling between the ground state and the excited state by the localised magnetic operators at the perimeter region of the solvated molecule. In contrast, the coupling is reduced for the carbon nuclei that are close to center. Another solvent-induced effect that originates from the magnetic anisotropy of the CH_3CN solvent molecules, was found to be small and almost constant.

Acknowledgements

The authors thank Mr. Jarkko Vähäkangas (Oulu) for technical assistance. Financial support was received from the Finnish Cultural Foundation (NÖ), Otto A. Malm Foundation (NÖ), the Academy of Finland (NÖ, JM, DS, JV), Tauno Tönning Fund (JV) and University of Oulu (JV). The work is part of the directed programme in Computational Science of the Academy of Finland. Computations were partially carried out at the CSC-IT Center for Science Ltd. (Espoo, Finland), and they benefitted also from the Finnish Grid Initiative (FGI) project.

References

1 C. P. Slichter, *Principles of Magnetic Resonance*, Springer, Berlin, 2nd edn, 1990.
2 M. Dračinský and P. Bouř, *J. Chem. Theor. Comput.*, 2010, **6**, 288–299.
3 A. Klamt and G. Schuurmann, *J. Chem. Soc., Perkin Trans. 2*, 1993, 799–805.
4 V. Barone, R. Improta and N. Rega, *Acc. Chem. Res.*, 2008, **41**, 605–616.
5 A. D. Buckingham, T. Schaefer and W. G. Schneider, *J. Chem. Phys.*, 1959, **32**, 1227.
6 D. B. Chesnut and B. E. Rusiloski, *J. Mol. Struct.: THEOCHEM*, 1994, **314**, 19 – 30.
7 V. G. Malkin, O. L. Malkina, G. Steinebrunner and H. Huber, *Chem. Eur. J.*, 1996, **2**, 452–457.
8 K. Modig, B. G. Pfrommer and B. Halle, *Phys. Rev. Lett.*, 2003, **90**, 075502.
9 T. S. Pennanen, J. Vaara, P. Lantto, A. J. Sillanpää, K. Laasonen and J. Jokisaari, *J. Am. Chem. Soc.*, 2004, **126**, 11093–11102.
10 T. S. Pennanen, P. Lantto, A. J. Sillanpää and J. Vaara, *J. Phys. Chem. A*, 2007, **111**, 182–192.
11 J. Kongsted, C. B. Nielsen, K. V. Mikkelsen, O. Christiansen and K. Ruud, *J. Chem. Phys.*, 2007, **126**, 034510.
12 R. Björnsson, H. Fruchtl and M. Bühl, *Phys. Chem. Chem. Phys.*, 2011, **13**, 619–627.
13 J. Asher and M. Kaupp, *Theor. Chem. Acc.*, 2008, **119**, 477–487.
14 S. Standara, P. Kulhánek, R. Marek and M. Straka, *J. Comput. Chem.*, 2013, **34**, 1890–1898.
15 S. Miertu, E. Scrocco and J. Tomasi, *Chem. Phys.*, 1981, **55**, 117 – 129.
16 K. Aidas, A. Møgelhøj, H. Kjær, C. B. Nielsen, K. V. Mikkelsen, K. Ruud, O. Christiansen and J. Kongsted, *J. Phys. Chem. A*, 2007, **111**, 4199–4210.
17 H. Fliegl, S. Taubert, O. Lehtonen and D. Sundholm, *Phys. Chem. Chem. Phys.*, 2011, **13**, 20500–20518.

18 K. V. Mikkelsen, K. Ruud and T. Helgaker, *Chem. Phys. Lett.*, 1996, **253**, 443 – 447.

19 M. Cossi, N. Rega, G. Scalmani and V. Barone, *J. Comput. Chem.*, 2003, **24**, 669–681.

20 J. Tomasi, B. Mennucci and R. Cammi, *Chem. Rev.*, 2005, **105**, 2999–3094.

21 T. S. Pennanen, P. Lantto, M. Hakala and J. Vaara, *Theor. Chem. Acc.*, 2011, **129**, 313–324.

22 M. P. Allen and D. J. Tildesley, *Computer Simulation of Liquids*, Clarendon Press, Oxford, 1987.

23 B. O'Regan and M. Grätzel, *Nature*, 1991, **353**, 737–740.

24 M. H. Levitt, *Spin Dynamics: Basics of Nuclear Magnetic Resonance*, Wiley, Chichester, 2001.

25 N. F. Ramsey, *Phys. Rev.*, 1950, **78**, 695–699.

26 N. F. Ramsey, *Phys. Rev.*, 1953, **91**, 303–307.

27 P. W. Atkins and R. S. Friedman, *Molecular Quantum Mechanics*, Oxford University Press, Oxford, 5th edn, 2011.

28 J. Vaara, K. Oikarinen, J. Jokisaari and J. Lounila, *Chem. Phys. Lett.*, 1996, **253**, 340 – 348.

29 M. Kühn, R. Send and D. Sundholm, *manuscript in preparation*.

30 J. Wang, W. Wang, P. A. Kollman and D. A. Case, *J. Mol. Graph. and Model.*, 2006, **25**, 247.

31 D. Case, T. Darden, I. T.E. Cheatham, C. Simmerling, J. Wang, R. Duke, R. Luo, R. Walker, W. Zhang, K. Merz, B. Roberts, S. Hayik, A. Roitberg, G. Seabra, J. Swails, A. Goetz, I. Kolossváry, K. Wong, F. Paesani, J. Vanicek, R. Wolf, J. Liu, X. Wu, S. Brozell, T. Steinbrecher, H. Gohlke, Q. Cai, X. Ye, J. Wang, M.-J. Hsieh, G. Cui, D. Roe, D. Mathews, M. Seetin, R. Salomon-Ferrer, C. Sagui, V. Babin, T. Luchko, S. Gusarov, A. Kovalenko and P. Kollman, *AMBER 12*, 2012.

32 M. J. S. Dewar and W. Thiel, *J. Am. Chem. Soc.*, 1977, **99**, 2338.

33 X. Grabuleda, C. Jaime and P. A. Kollman, *J. Comput. Chem.*, 2000, **21**, 901.

34 J. C. Phillips, R. Braun, W. Wang, J. Gumbart, E. Tajkhorshid, E. Villa, C. Chipot, R. D. Skeel, L. Kalé and K. Schulten, *J. Comput. Chem.*, 2005, **26**, 1781.

35 C. Lee, W. Yang and R. G. Parr, *Phys. Rev. B*, 1988, **37**, 785–789.

36 A. D. Becke, *J. Chem. Phys.*, 1993, **98**, 5648–5652.

37 P. J. Stephens, F. J. Devlin, C. F. Chabalowski and M. J. Frisch, *J. Phys. Chem.*, 1994, **98**, 11623–11627.

38 F. Weigend and R. Ahlrichs, *Phys. Chem. Chem. Phys.*, 2005, **7**, 3297–3305.

39 H. Flyvbjerg and H. G. Petersen, *J. Chem. Phys.*, 1989, **91**, 461–466.

40 H. H. Schäfer and R. Ahlrichs, *J. Chem. Phys.*, 1992, **97**, 2571–2577.

41 R. Ahlrichs, M. Bär, M. Häser, H. Horn and C. Kölmel, *Chem. Phys. Lett.*, 1989, **162**, 165–169.

42 Z. L. Terranova and S. A. Corcelli, *J. Phys. Chem. B*, 2013, **117**, 15659–15666.

43 J. Vaara, *Phys. Chem. Chem. Phys.*, 2007, **9**, 5399–5418.

44 J. L. M. Abboud, A. Auhmani, H. Bitar, M. El Mouhtadi, J. Martin and M. Rico, *J. Am. Chem. Soc.*, 1987, **109**, 1332–1341.

45 C. Eckart, *Phys. Rev.*, 1935, **47**, 552–558.

46 J. Vaara, J. Lounila, K. Ruud and T. Helgaker, *J. Chem. Phys.*, 1998, **109**, 8388–8397.

47 O. Lehtonen, D. Sundholm, R. Send and M. P. Johansson, *J. Chem. Phys.*, 2009, **131**, 024301.

48 M. E. Casida, C. Jamorski, K. C. Casida and D. R. Salahub, *J. Chem. Phys.*, 1998, **108**, 4439–4449.

49 C.-O. Almbladh and U. von Barth, *Phys. Rev. B*, 1985, **31**, 3231–3244.